Kesaria, M. , Alshahrani, D., Kwan, D., Anyebe, E. and Srivastava, V. 2021. Optical and electrical performance of 5 µm InAs/GaSb Type-II superlattice for NOx sensing application. Materials Research Bulletin 142 , 111424. 10.1016/j.materresbull.2021.111424

Publishers page: http://dx.doi.org/10.1016/j.materresbull.2021.1114...

Optical and electrical performance of 5 μm InAs/GaSb Type-II superlattice for NOx sensing application

M Kesaria , D Alshahrani , D Kwan , E Anyebe , V Srivastava

PII: S0025-5408(21)00221-X
DOI: https://doi.org/10.1016/j.materresbull.2021.111424
Reference: MRB 111424

To appear in: *Materials Research Bulletin*

Received date: 17 January 2021
Revised date: 17 May 2021
Accepted date: 19 May 2021

Please cite this article as: M Kesaria , D Alshahrani , D Kwan , E Anyebe , V Srivastava , Optical and electrical performance of 5 μm InAs/GaSb Type-II superlattice for NOx sensing application, *Materials Research Bulletin* (2021), doi: https://doi.org/10.1016/j.materresbull.2021.111424

Highlights

- Environmental pollutant NOx is the greatest global challenge confronting humanity
- Optical properties and electrical properties of 5 µ InAs/GaSb T2SL photodiode
- Higher operating temperature (200 -300 K), G-R and TAT are dominant
- Surface leakage contributes to G-R dark current in T2SL photodiodes

Optical and electrical performance of 5 µm InAs/GaSb Type-II superlattice for NOx sensing application

M Kesaria*, D Alshahrani, D Kwan, E Anyebe and V Srivastava

School of Physics and Astronomy, Cardiff University, Cardiff.

Abstract

We report on the optical and electrical performance of optimized InAs/GaSb type-II superlattice (T2SL). The optical quality of optimal T2SL is compared with InAs/InAsSb T2SL. Dominant photoluminescence (PL) peak at around 5.3µm at 77 K was obtained for the Ga-based samples with an intensity which is less sensitive to changes in temperature compared to the Ga-free SL. The PL peak intensity of the Ga-based T2SL with an intentional InSb layer was found to be less responsive to changes in temperature and tuned to longer wavelength suitable for NO_x sensing. Current-Voltage modelling of the fabricated Photodiode demonstrates that at a temperature of 110K, generation recombination (G-R) and trap assisted tunnelling (TAT) currents dominates below and above an applied bias of ~0.2 V respectively. However, at higher operating temperature (200 -300 K), diffusion current is prevalent at low applied bias while G-R and TAT are dominant at high applied bias.

Keywords: A. InAs/GaSb, A. Type-II superlattice, D. 5 µm, D. photodiodes, D. NO_x sensing

***corresponding author email:** kesariam@cardiff.ac.uk.

Introduction

Environmental pollution is one of the greatest challenges confronting humanity globally. Nitric oxide (NO) and nitrogen dioxide (NO_2), which are collectively referred to as NOx, are highly poisonous and detrimental to air quality and a primary source of air pollution, contributing to the formation of smog and acid rain[1]. NOx is a toxic gas produced during combustion of fossil fuels in power plants and automobile engines as well as during lightning in thunderstorms and contributes to numerous functions in the human body where it is produced in inflammatory processes [**2-4**]. Traditional gas detection instruments, such as chemiresistive sensors, require direct contact with the target gas, greatly limiting their practical use for scanning of large areas or multiple sites. However, by making use of the unique absorption spectra of NOx gases, optical gas detectors can provide real time imaging in which target gases appear as highlighted clouds. Therefore, non-contact, photodetector-based sensors are both faster and more practical than conventional gas detectors for most industrial applications.

Highly sensitive photodetectors operating in the 5.1 - 5.6 µm spectra band at high temperature are urgently required for low-cost detection of NOx gas. Although, Mercury Cadmium Telluride (MCT) and Quantum Well Infrared Photodetectors (QWIPs) are well-established technologies in mid-infrared (MWIR) for photodetection. They require cryogenic cooling systems to achieve high signal-to-noise ratio at high temperatures. In addition, MCT is plagued with high material toxicity [5, 6], poor uniformity [6, 7], fabrication complexity, high cost and low producibility yield while QWIPs suffers from low quantum efficiency, lower operating temperature [8] and one-dimensional (1 D) carrier confinement which increases dark current making them unsuitable for high-temperature operation **[9-11].** Type-II superlattices (T2SL) have emerged as a promising alternative to MCT and QWIPs due to their flexible and more controllable band-gap engineering through the design of the SL layer thickness/composition and coherency strain[12]. However, recent atom probe tomography and X-ray energy dispersive spectrometry studies [13, 14] have demonstrated that Ga-free InAs/InAsSb T2SL exhibit Sb segregation which could potentially induce undesirable effects on band-gap engineering including broadening of the optical response, as well as weakened absorption[12]. Consequently, Ga-based InAs/GaSb T2SL infrared material have attracted extensive research interest for photodetection due to their potential to provide cheaper, high device performance at high temperature with significantly reduced dark current[15] and high responsivity[11] resulting from large absorption coefficient[16], reduced tunnelling currents[17] and reduced hole–hole auger recombination due to the large splitting between the heavy-hole and the light-hole bands of the superlattice[18]. InAs/GaSb T2SL have been theoretically predicted[7, 19] to significantly outperform current state-of-the-art MCT.

There are limited reports[20, 21] of near room temperature photodetection using InAs/GaSb SL within the 5.1 - 5.6 µm spectra window for NO_x detection. Rogalski et al [20] achieved 50% cut-off wavelength of 5.2µm at 230 K on a T2SL InAs/GaSb mesa PIN architecture using GaAs substrate converted into immersion lens for increased detectivity. Krishna et al [21] obtained a cut off wavelength of 5.2µm at room temperature using a nBn structure based on InAs/GaSb T2SL. It is essential to further extend the detection limit of InAs/GaSb T2SL towards 5.5µm at near room temperature. More so, there is very limited detailed investigation [22] of the temperature-dependent PL investigation of InAs/GaAs SL as such there is a need for further research activities to better understand the optical properties at higher operating temperature. In a previous study [23], we have investigated the influence of the shutter sequence during the growth of InAs/GaSb SL on the structural, morphological and optical properties at 77K. In this study, we report the optical and electrical characteristics of 5.5µm *nip* InAs/GaSb T2SL layers and photodiodes operating up to 300K.

Experimental method

To investigate the optical properties of MWIR Ga-based T2SLs, two InAs/GaSb SL samples were grown by molecular beam epitaxy (MBE) at optimized condition[20]. Sample A was grown with an intentional InSb layer grown using migration enhanced epitaxy (MEE) at both interfaces while sample B was grown using an antimony-for-arsenic exchange at the GaSb-on-InAs IF leading to an 'InSb-like' interfaces (IFs). **Figure 1** shows the schematic diagrams of the samples. More details of the growth method of these samples can be found elsewhere[23]. Both samples were grown on GaSb substrates with GaSb buffer layers and thicknesses of 50 nm. The samples consist of 100 periods of a superlattice with the asymmetrical layer thicknesses of 7 MLs of InAs and 4 MLs of GaSb in every single period. Both samples were then capped with 1.2 nm of GaSb layers. Growth details of the Ga-free InAs/InAsSb SL reference (sample C) could be found elsewhere [25, 26]. The optical characteristics of both samples were investigated by PL measurements at different temperatures from 77 K to 293 K. A Nicolet iS50R Fourier Transform Infrared (FTIR) Spectrometer was used to acquire PL signal from the samples. The samples were loaded into a

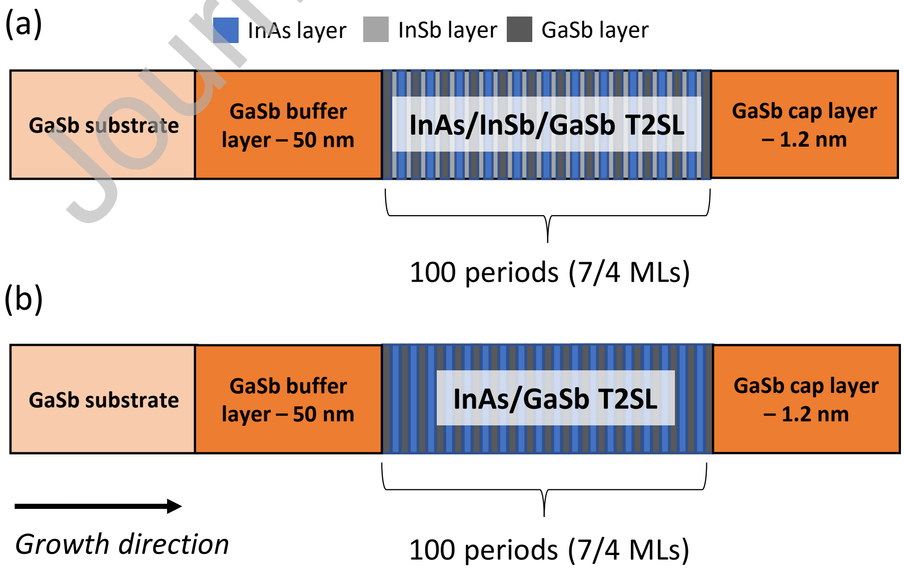

Figure 1. A schematic diagram shows the Ga-based T2SL samples grown by MBE using (a) MEE method (sample A) and (b) As-Sb exchange growth technique (sample B) and used to undertake PL measurements.

cryostat supplied with CaF_2 windows to perform temperature-dependent PL measurements using liquid nitrogen. A laser diode with a wavelength of 785 nm was used as an excitation source and the excitation power of the laser was fixed to ~50 mW. A cooled MCT detector with a high detectivity was utilised as a detector source for the PL signal. A *nip* photodiode with an intrinsic region similar to sample B was grown using the same growth conditions described above. Photodiodes were fabricated using a standard photolithography process. Cr/Au contacts were evaporated onto the top and bottom of the sample and a citric acid-based wet etch was used to define 90 to 440 µm diameter mesas. Photoresist protection was used to block the mesa sidewalls from ambient air. A schematic of a fabricated nip detector, and the current path therein, is shown in **Figure 2**. Liquid nitrogen cooled cryogenic probe station was then used to perform current-voltage measurements on a 140 µm diode.

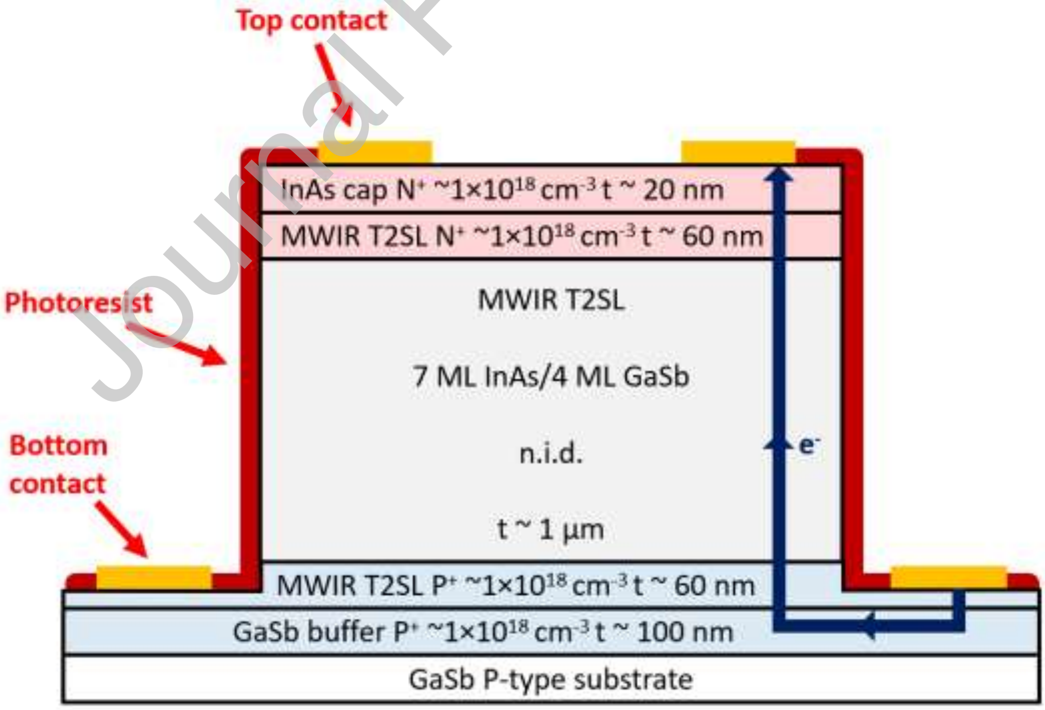

Figure 2: A schematic representation of a fabricated nip diode. Blue arrows highlight the flow of electrons.

Results and discussion

Material characterization, including X-ray diffraction (XRD) ω/2θ scans and Atomic Force Microscopy (AFM), were performed for Samples A and B and reported in a previous work [23]. Sample A was found to be under slight compressive strain, indicating the total thickness of the InSb IFs is too large. The SL layers of Sample B were found to be almost lattice matched onto the GaSb substrate. The slight lattice mismatch in Sample B may have led to a minor degradation in material quality which is corroborated by a slightly larger XRD FWHM and rms roughness as measured by AFM.

Figure 3 shows the temperature-dependent PL spectra of the Ga-based samples. At 77 K, the dominant PL peak energies are positioned at around 5.3µm, for both samples [5.5µm (225meV) and 5.1 µm (243meV) for samples A and B respectively]. This dominant PL peak is associated with the SL transition energy from the first electron miniband to the heavy hole miniband (e_1-hh_1). The observed redshift in the peak position of sample A relative to B is attributed to the presence of the relatively thick InSb IF layer at the SL interfaces of sample A [23] which contributes to a decrease in PL peak energy consistent with a previous study [27]. The 50% cut-off wavelength at 77 K for each sample, here defined as the energy value of the negative slope of the PL profile at half maximum intensity, was measured to be 0.240 eV and 0.259 eV for Samples A and B, respectively. These measurements confirm the suitability of the T2SLs for NO_x sensing applications.

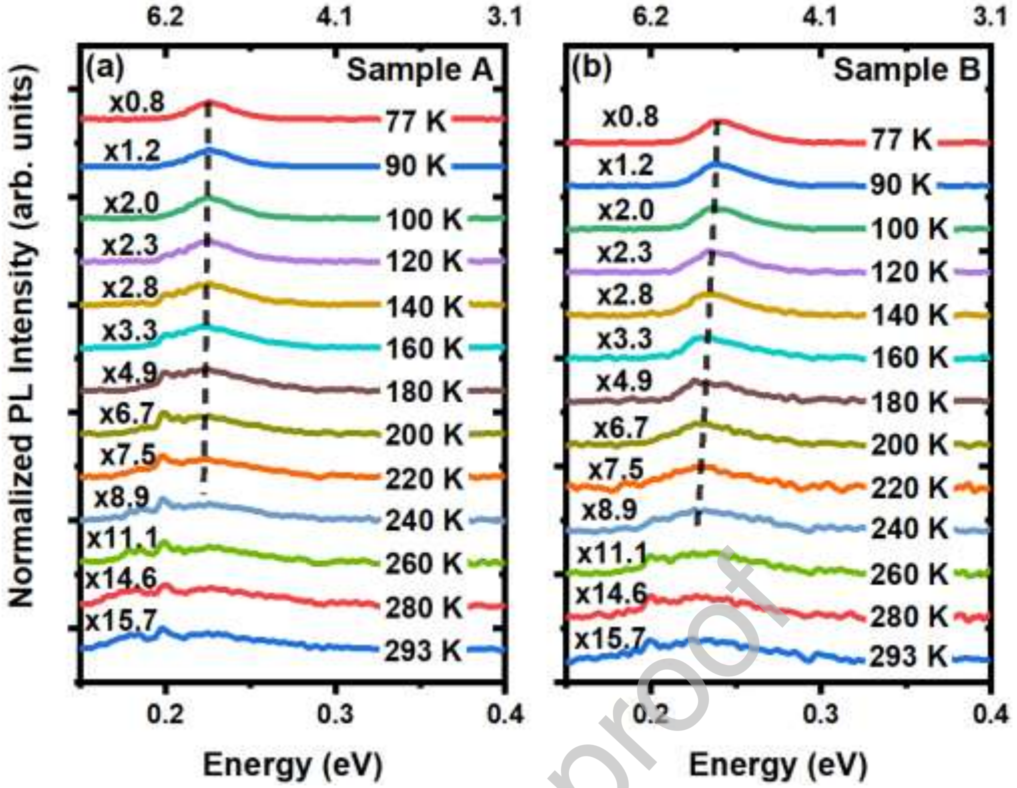

Figure 3. Normalized temperature dependant PL spectra of both Samples A and B.

Excitons are thermally excited from the first miniband electrons to the conduction band of the InSb-like interfaces to recombine non-radiatively [28, 29]. A redshift of 22 and 19 meV with increasing temperature from 77 to 293 K was obtained for samples A and B respectively. As expected, the PL peak intensity of both samples decreases with increasing temperature.

A Gaussian fitting analysis was used to extract the band energy from **Figure 3** as a function of temperature, the results are shown in **Figure 4(a).** The temperature dependant behaviour of the band energy was fitted using the well-known Varshni equation[30]:

$$\boldsymbol{E_g(T) = E_g(0K) - \frac{\alpha.T^2}{\beta+T}}, \quad \textbf{(1)}$$

Where E_g is the band gap energy, T is the temperature and α and β are fitting parameters. The value of β was fixed at 270 K in accordance with a previous report[31]. The α values were thusly determined to be 0.162 meV and 0.171 meV for Samples A and B, respectively, which is close to that of a previously reported MWIR InAs/GaSb T2SL detector[32]. The integrated PL intensities of the samples are compared to that of a reference Ga- free, InAs/InAsSb T2SLs (sample C) as shown in **Figure 4(b).** Gradients of (3.22± 1.92, 3.67± 2.45 and 6.00± 7.83) x 10^{-3} for samples A, B and C respectively were extracted. The gradient of the Ga-free SL almost twice that of the Ga-based one for similar temperature regime which indicates that the two Ga-based samples are less sensitive to temperature than the Ga-free SL reference sample C. The relatively low rate of quenching of the Ga-based samples could be related to the presence of fewer non-radiative defects centres corresponding to a lower rate of thermal quenching[33]. In addition, compared to the rapid thermal quenching of the PL intensity of sample B, sample A is less sensitive to temperature changes with its PL intensity quenched by only about half of that of sample B for changes in temperature in the interval 77 - 293 K (see also **Figure 3**) which suggests the presence of more non-radiative recombination centres in sample B. This demonstrates the superior optical property of sample A grown with an intentional InSb layer compared to sample B in good agreement with a previous study[34] and attributed to the smoother surface at the interface.

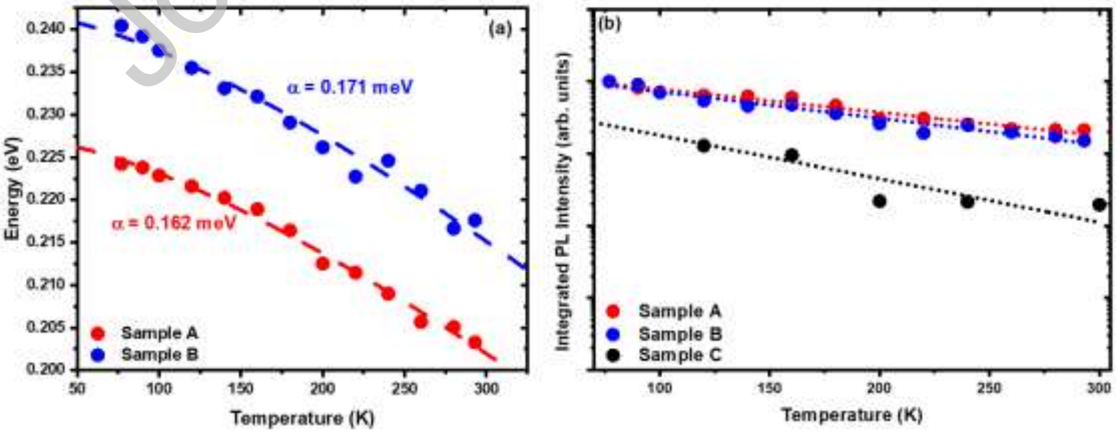

Figure 4. (a) The measured band energy for Samples A and B as a function of temperature, fitted using the Varshni equation. (b) Temperature dependant integrated PL intensity for Samples A, B, and C.

The 8-band **k·p** envelope-function method implemented in the Nextnano3 software [35] was employed to model the band structure of the 7 ML InAs/4 ML GaSb T2SL which is depicted in **Figure 5**. (Details of the parameters used can be found elsewhere[36]). It should be noted that Sample A was modelled as having an InSb interfacial layer at both IFs while Sample B was modelled as having an InSb layer at the GaSb-on-InAs layer and a sharp IF at the InAs-on-GaSb IF. Interestingly, the calculated energy gap of 225meV for sample A is consistent with that predicted by the PL result and redshifted with respect to the simulated band energy of Sample B (237meV), as earlier demonstrated by PL result, but is slightly off the measured band energy.

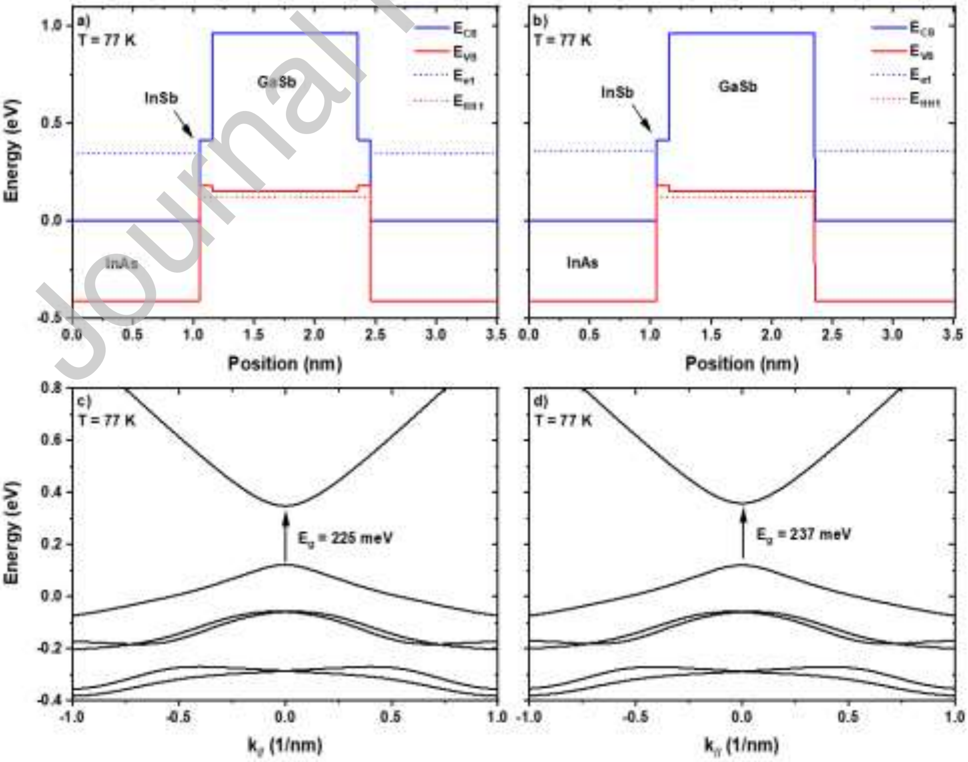

Figure 5: (a) Schematic diagram of the simulated band structure of the 7/4 SL for samples A and B (a-b) respectively. The electronic band structure of a 7/4 SL calculated at T = 77K for two in-plane directions in the Brillouin zone for sample A and B (c-d) respectively.

This can be attributed to the uncertainty of the composition of the IFs, particularly the InAs-on-GaSb IF. This further indicates that the band energy of the InAs/GaAs SL could be tuned to longer wavelength with the insertion of InSb layer at both interfaces. The electronic band structure of the 7/4 SL calculated at T = 77K for two in-plane directions in the Brillouin zone for samples A and B are shown in Figure 4c-d, respectively.

Figure 6a shows the temperature-dependent current density characteristics of the nip photodetectors at 110 K, 200 K and 300 K. As expected, the dark current density increases

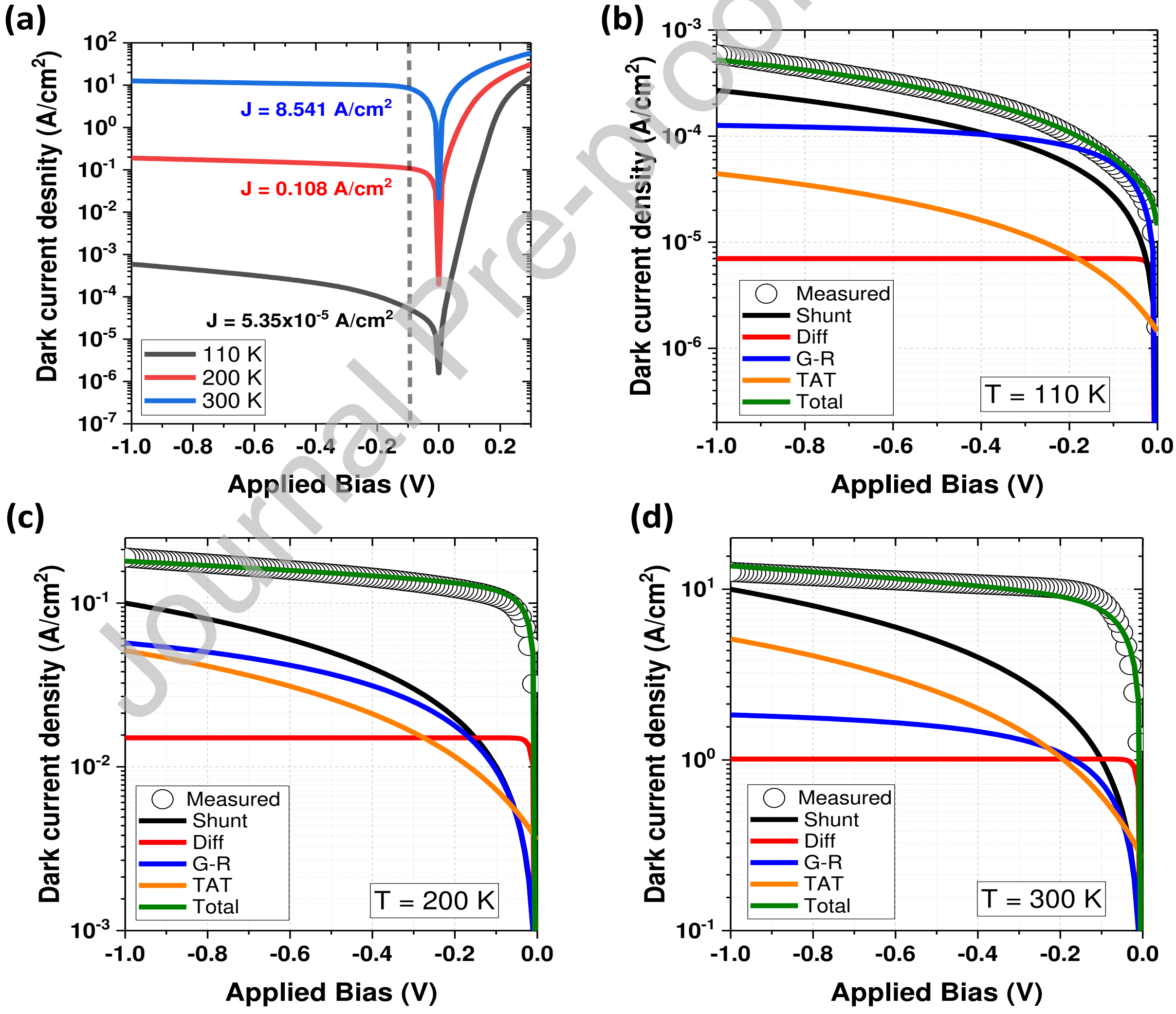

Figure 6: (a) Measured dark current density vs applied bias characteristics of the photodetectors at temperatures 110, 200, and 300 K. Modelled dark current density under applied bias at temperatures of (b) 110 K, (c) 200 K, (d) 300 K.

from 5.35x 10^{-5} to 8.541 A/cm^2 as the temperature was increased from 110 to 300 K. The modelled dark current density under reverse bias at different temperatures is shown in **Figures 6 b-d**. The dark current in a T2SLs diode has been accurately modelled by Gopal et al. [37-38] to be the sum of diffusion, trap assisted tunnelling (TAT), shunt and generation-recombination (G-R) current. Diffusion current refers to the diffusion of minority carriers from high to low concentrations and can be modelled as:

$$I_{diff} = \frac{qAn_i^2}{N_d}\left\{\frac{kT}{q}\frac{\mu_h}{\tau_h}\right\}^{1/2}\tanh\frac{d}{L_h}\left[\exp\left(\frac{qV}{kT}\right)-1\right], \quad (1)$$

where N_d is the donor concentration, n_i is the intrinsic carrier concentration, A is the junction area, V is the diode bias voltage, d is the thickness of the n region, τ_h is the hole lifetime, μ_h is the hole mobility and L_h is the hole diffusion length. G-R current is related to defects in the depletion region acting as Shockley-Read-Hall (SRH) recombination centres. For reverse bias, considered above, the G-R current can be given by:

$$I_{G-R} = \frac{qAn_iW_{dep}V}{V_t\tau_{G-R}}, \quad (2)$$

$$A_{G-R} = \frac{qn_tA}{2\tau_{G-R}}\left[\frac{2\varepsilon_0\varepsilon_s(N_a+N_d)}{qN_aN_d}\right]^{1/2}, \quad (3)$$

where τ_{G-R} is the G-R lifetime, N_a is the acceptor concentration and W_{dep} is the depletion region width. The TAT current originates from mid-gap trap states which carriers can use to tunnel between bands, usually under a high electric field, and is expressed as:

$$I_{TAT} = \frac{\pi^2q^2Am_eV_tM^2N_T}{h^3(E_g-E_t)}\times\exp\left\{-\frac{8\pi(2m_e)^{1/2}(E_g-E_t)^{3/2}}{[3qhF(V)]}\right\}, \quad (4)$$

where m_e is the tunnelling effective mass, E_g is the superlattice bandgap, h is Planck's constant, M is the matrix element associated with the trap potential, F(V) is the voltage dependant electric field strength across the depletion region, E_t is the location of the trap level below the conduction band edge, N_T is the trap density. Ohmic shunt currents are usually caused by native oxides, formed on the mesa sidewalls during etching, which act as good conductors. This component can simply be described using Ohm's law:

$$I_{sh} = \frac{V}{R_{sh}}, \tag{5}$$

where R_{sh} is the diode shunt resistance. Due to the limited shielding of the probe station, a measurement temperature of 110 K was chosen to negate the effect of photocurrent. This model fits the data well except for a small deviation at high bias which can be attributed to the band-to-band tunnelling current not considered here. **Figure 6b** shows that at a relatively low temperature of 110K, G-R current is dominant at low applied bias, but TAT current dominates when the bias is increased above ~0.2 V. However, at higher operating temperatures of 200 and 300 K, the contribution of diffusion current becomes dominant at low applied bias ~50 mV while G-R and TAT dominate the current at bias above ~0.2 V. This result is consistent with results of similar devices which are G-R limited at low temperatures [40, 41]. The significant contribution of the shunt current can be attributed to the lack of passivation.

Conclusion

In this paper, the optical properties of the two grown Ga-based InAs/GaSb T2SL samples were explored using temperature-dependent photoluminescence measurements. It has been shown that incorporation of intentional InSb layers at the interfaces between InAs and GaSb SL layers for sample A results in a redshift in the PL wavelengths compared to sample B. Also, it has been shown that sample A is much less sensitive to temperature changes with its PL intensities quenched by only about half of that of sample B for changes in temperature in the interval 77 - 293 K. To examine the electrical performance of the fabricated *nip* photodiodes, I-V measurements were carried out and modelled at 110, 200 and 300K. From the JV modelling, it has been shown that G-R mechanism is the main source of dark current at low reverse bias, while TAT is dominant at an applied bias above ~0.2 V. However, at higher operating temperature (200 -300 K), diffusion current is prevalent at low applied bias while G-R and TAT dominate for high applied bias. Also, the shunt current has a considerable contribution to the dark current over the whole applied bias range which could be attributed to the lack of surface passivation. This study demonstrates that InAs/GaSb Type-II superlattice are highly promising for NOx sensing at around 5 µm. However, the optical and electrical properties of the InAs/GaSb T2SL could be further improved by applying surface passivation processes to minimize the contribution of G-R dark current and enhance the overall dark current of the photodiodes.

Author's Statement

We the undersigned declare that this manuscript is original, has not been published before and is not currently being considered for publication elsewhere.

We wish to confirm that there are no known conflicts of interest associated with this publication and there has been no significant financial support for this work that could have influenced its outcome.

We confirm that the manuscript has been read and approved by all named authors and that there are no other persons who satisfied the criteria for authorship but are not listed.

We further confirm that the order of authors listed in the manuscript has been approved by all of us.

We confirm that we have given due consideration to the protection of intellectual property associated with this work and that there are no impediments to publication, including the timing of publication, with respect to intellectual property. In so doing we confirm that we have followed the regulations of our institutions concerning intellectual property.

We understand that the Corresponding Author is the sole contact for the Editorial process (including Editorial Manager and direct communications with the office). He is responsible for communicating with the other authors about progress, submissions of revisions and final approval of proofs.

We confirm that we have provided a current, correct email address which is accessible by the Corresponding Author and which has been configured to accept email.

Signed by all authors as follows:

M kesaria, Ph.D., kesariam@cardiff.ac.uk

D Alshahrani, alshahranid@cardiff.ac.uk

D Kwan, KwanDC@cardiff.ac.uk

E Anyebe, PhD, AnyebeE@cardiff.ac.uk

V Srivastava, PhD, srivastavaV6@cardiff.ac.uk

Declaration of interests

☒ The authors declare that they have no known competing financial interests or personal relationships that could have appeared to influence the work reported in this paper.

References

[1] R.J. Hargreaves, I.E. Gordon, L.S. Rothman, S.A. Tashkun, V.I. Perevalov, A.A. Lukashevskaya, S.N. Yurchenko, J. Tennyson, H.S.P. Muller, Spectroscopic line parameters of NO, NO_2, and N_2O for the HITEMP database, J Quant Spectrosc Radiat Transf. 232 (2019) 35-53.

[2] J. Wojtas, A. Gluszek, A. Hudzikowski, F.K. Tittel, Mid-Infrared Trace Gas Sensor Technology Based on Intracavity Quartz-Enhanced Photoacoustic Spectroscopy, Sensors 17 (2017) 513.

[3] L.Yang, , Li. L., Y. Yang, G. Zhang, L. Gong, L. Jing, H. Fu and K. Shi (2013). Facile synthesis of Cu/Cu_xO nanoarchitectures with adjustable phase composition for effective NO_x gas sensor at room temperature. Materials Research Bulletin 48 (2013) 3657-3665.

[4] Yan, D., S. Xia, S. Li, S. Wang, M. Tan and S. Liu "Electrophoretic deposition of multiwalled carbon nanotubes onto porous silicon with enhanced NO2-sensing characteristics." Materials Research Bulletin 134 (2021) 111109.

[5] A. Rogalski, P. Martyniuk, M. Kopytko, Challenges of small-pixel infrared detectors: A Review, Rep. Prog. Phys. 79 (2016) 046501.

[6] A. Rogalski, Infrared detectors: status and trends, Prog. Quantum. Electron 27 (2003) 59-210.

[7] G.A. Umana-Membreno, B. Klein, H. Kala, J. Antoszewski, G. Gautam, M.N. Kutty, E. Plis, J.M. Dell, S. Krishna, L. Faraone, Vertical transport in InAs/GaSb type-II strained-layer superlattices for infrared focal plane array applications, Proc. SPIE 8012, Infrared Technology and Applications XXXVII, 80120Y (20 May 2011).

[8] A.M. Hoang, A. Dehzangi, S. Adhikary, M. Razeghi, High performance bias-selectable three-color Short-wave/Mid-wave/Long-wave Infrared Photodetectors based on Type-II InAs/GaSb/AlSb superlattices, Sci. Rep. 6 (2016) 24144.

[9] Aulombard, R. L. and A. Joullie "Melt growth and some electrical properties of GaSb AlSb system." Materials Research Bulletin 14(1979) 349-359.

[10] C. Popescu, Semiconductor superlattices and interfaces: Edited by A. Stella and L. Miglio. Elsevier Science Publishers, Amsterdam (1993), 490 pp. Materials Research Bulletin 29(1994) 459-460.

[11] M.J. Hobbs, F. Bastiman, C.H. Tan, J.P.R. David, S. Krishna, E. Plis, Uncooled MWIR InAs/GaSb type-II superlattice grown on a GaAs substrate, Proc. SPIE 8899, Emerging Technologies in Security and Defence; and Quantum Security II; and Unmanned Sensor Systems X, 889906 (16 October 2013)

[12] J. Lu, E. Luna, T. Aoki, E.H. Steenbergen, Y.H. Zhang, D.J. Smith, Evaluation of antimony segregation in InAs/InAs1-xSbx type-II superlattices grown by molecular beam epitaxy, J. Appl. Phys. 119 (2016) 095702.

[13] N.A. Kotulak, J.A. Nolde, M.B. Katz, M.E. Twigg, K.E. Knipling, D. Lubyshev, J.M. Fastenau, A.W.K. Liu, E.H. Aifer, Three-dimensional visualization of Sb segregation in InAs/InAsSb superlattices using atom probe tomography, J. Appl. Phys.128 (2020) 015302.

[14] H.J. Haugan, K. Mahalingam, F. Szmulowicz, G.J. Brown, Quantitative study of the effect of deposition temperature on antimony incorporation in InAs/InAsSb superlattices, J. Cryst. Growth 436 (2016) 134-137.

[15] A. Rogalski, Recent progress in infrared detector technologies, Infrared Phys Technol. 54 (2011) 136-154.

[16] H.J. Haugan, F. Szmulowicz, G.J. Brown, K. Mahalingam, Band gap tuning of InAs/GaSb type-II superlattices for mid-infrared detection, J. Appl. Phys. 96 (2004) 2580-2585.

[17] H. Mohseni, V.I. Litvinov, M. Razeghi, Interface-induced suppression of the Auger recombination in type-II InAs/GaSb superlattices, Phys. Rev. B 58 (1998) 15378-15380.

[18] C.H. Grein, W.H. Lau, T.L. Harbert, M.E. Flatte, Modeling of very long infrared wavelength InAs/GaInSb strained layer superlattice detectors, Proc. SPIE 4795, Materials for Infrared Detectors II, (5 December 2002).

[19] A. Rogalski, New material systems for third generation infrared photodetectors, Opto-Electronics Review 16 (2008) 458-482.

[20] P. Martyniuk, D. Benyahia, A. Kowalewski, L. Kubiszyn, D. Stepien, W. Gawron, A. Rogalski, Mid-wave T2SLs InAs/GaSb single pixel PIN detector with GaAs immersion lens for HOT condition, Solid-State Electron 119 (2016) 1-4.

[21] J.B. Rodriguez, E. Plis, G. Bishop, Y.D. Sharma, H. Kim, L.R. Dawson, S. Krishna, nBn structure based on InAs/GaSb type-II strained layer superlattices, App. Phys. Lett. 91 (2007) 043514.

[22] C. Cervera, J.B. Rodriguez, J.P. Perez, H. Ait-Kaci, R. Chaghi, L. Konczewicz, S. Contreras, P. Christol, Unambiguous determination of carrier concentration and mobility for InAs/GaSb superlattice photodiode optimization, J. Appl. Phys.106 (2009) 033709.

[23] M. Delmas, M.C. Debnath, B.L. Liang, D.L. Huffaker, Material and device characterization of Type-II InAs/GaSb superlattice infrared detectors, Infrared Phys Technol. 94 (2018) 286-290.

[24] R. Taalat, J.B. Rodriguez, M. Delmas, P. Christol, Influence of the period thickness and composition on the electro-optical properties of type-II InAs/GaSb midwave infrared superlattice photodetectors, J. Phys. D: Appl. Phys. 47 (2014) 015101.

[25] J.A. Keen, E. Repiso, Q. Lu, M. Kesaria, A.R.J. Marshall, A. Krier, Electroluminescence and photoluminescence of type-II InAs/InAsSb strained-layer superlattices in the mid-infrared, Infrared Phys Technol. 93 (2018) 375-380.

[26] J.A. Keen, D. Lane, M. Kesaria, A.R.J. Marshall, A. Krier, InAs/InAsSb type-II strained-layer superlattices for mid-infrared LEDs, J. Phys. D: Appl. Phys. 51 (2018) 075103.

[27] J.B. Rodriguez, P. Christol, L. Cerutti, F. Chevrier, A. Joullie, MBE growth and characterization of type-II InAs/GaSb superlattices for mid-infrared detection, J. Cryst. Growth 274 (2005) 6-13.

[28] X.R. Chen, Y. Zhou, L. Zhu, Z. Qi, Q.Q. Xu, Z.C. Xu, S.L. Guo, J.X. Chen, L. He, J. Shao, Evolution of interfacial properties with annealing in InAs/GaSb superlattice probed by infrared photoluminescence, Jpn J Appl Phys. 53 (2014) 082201.

[29] J. Wu, Z.C. Xu, J.X. Chen, L. He, Temperature-dependent photoluminescence of the InAs-based and GaSb-based type-II superlattices, Infrared Phys Technol. 92 (2018) 18-23.

[30] P. Y. Varshni, Temperature dependence of the energy gap in semiconductors, Physica, 34 (1967) 149-154

[31] G. Klein, E. Plis, M. N. Kuttym N. Gautam, A. Albrecht, S. Meyers, and S. Krishna, J. Phys. D. Appl. Phys. 44 (2011) 075102

[32] P. Martyniuk, J. Wrobel, E. Plis, P. Madejczyk, W. Gawron, A. Kowalewski, S. Krishna, A. Rogalski, Proc. SPIR Optical Engineering, 52 (2013) 061307

[33] W. Pickin, J.P.R. David, Carrier decay In GaAs Quantum Wells, App. Phys. Lett. 56 (1990) 268-270.

[34] Z.C. Xu, J.X. Chen, F.F. Wang, Y. Zhou, Q.Q. Xu, C. Jin, H. Li, Interface design and properties in InAs/GaSb type-II superlattices grown by molecular beam epitaxy, Proc. SPIE 8907, International Symposium on Photoelectronic Detection and Imaging 2013: Infrared Imaging and Applications, 89073J (11 September 2013).

[35] Nextnano nextnano3 software www.nextnano.de/nextnano3/.

[36] M. Delmas, B.L. Liang, D.L. Huffaker, A comprehensive set of simulation tools to model and design high performance Type-II InAs/GaSb superlattice infrared detectors, Proc. SPIE 10926, Quantum Sensing and Nano Electronics and Photonics XVI, 109260G (1 February 2019).

[37] V. Gopal, S. Gupta, R.K. Bhan, R. Pal, P.K. Chaudhary, V. Kumar, Modeling of dark characteristics of mercury cadmium telluride n(+)-p junctions, Infrared Phys Technol. 44 (2003) 143-152.

[38] V. Gopal, E. Plis, J.B. Rodriguez, C.E. Jones, L. Faraone, S. Krishna, Modeling of electrical characteristics of midwave type II InAs/GaSb strain layer superlattice diodes, J. Appl. Phys. 104 (2008) 124506.

[39] V. Gopal, N. Gautam, E. Plis, S. Krishna, Modelling of current-voltage characteristics of infrared photo-detectors based on type - II InAs/GaSb super-lattice diodes with unipolar blocking layers, Aip Adv. 5 (2015) 097132.

[40] L. Ciura, A. Kolek, J. Wrobel, W. Gawron, A. Rogalski, 1/f Noise in Mid-Wavelength Infrared Detectors With InAs/GaSb Superlattice Absorber, IEEE Transactions on Electron Devices 62 (2015) 2022-2026.

[41] P. Christol, C. Cervera, J.B. Rodriguez, K. Jaworowicz, I. Ribet-Mohamed, Asymmetric InAs/GaSb superlattice pin photodiode to improve temperature operation, Proc. SPIE 7945, Quantum Sensing and Nanophotonic Devices VIII, 79451H (24 January 2011).

Graphical Abstract